Modular Organization of Axial Microcircuits in Zebrafish

Martha W. Bagnall and David L. McLean*

Locomotion requires precise control of spinal networks. In tetrapods and bipeds, dynamic regulation of locomotion is simplified by the modular organization of spinal limb circuits, but it is not known whether their predecessors, fish axial circuits, are similarly organized. Here, we demonstrate that the larval zebrafish spinal cord contains distinct, parallel microcircuits for independent control of dorsal and ventral musculature on each side of the body. During normal swimming, dorsal and ventral microcircuits are equally active, but, during postural correction, fish differentially engage these microcircuits to generate torque for self-righting. These findings reveal greater complexity in the axial spinal networks responsible for swimming than previously recognized and suggest an early template of modular organization for more-complex locomotor circuits in later vertebrates.

Animals make effective progress through unpredictable environments by rapidly adjusting ongoing locomotor movements (*1*, *2*). In limbed vertebrates, spinal microcircuits are organized into modules for efficient coordination of joints, limbs, and trunk during locomotion (*3*, *4*). However, it is unknown how the modular organization of complex spinal circuitry in tetrapods and bipeds could have arisen from the simpler, ancestral axial network of fish (*5*). Current models of axially based locomotion in fish engage left-right alternation circuits but do not include equivalent ipsilaterally organized microcircuits akin to those seen in higher vertebrates (*6*). Instead, it is thought that differential activation of dorsal and ventral musculature for behaviors such as postural control is achieved by supraspinal descending commands (*7*). To address this gap, we explored whether axial circuitry in fish contains more complexity than previously recognized.

In larval zebrafish, as with adults, swimming is produced by the left-right alternation of axial muscles activated in waves by segmentally iterated pools of motor neurons (MNs). In each spinal hemisegment is a cohort of four early-developing "primary" MNs, whose axon arborizations collectively tile the dorsal and ventral musculature (Fig. 1H) (*8*, *9*). Because all primary MNs exhibit identical recruitment patterns during swimming (*9*, *10*), there should be no confounding effects of speed-dependent differences on the configuration of their premotor circuits (*11*). Thus, current models would predict that they are embedded in a shared premotor network.

To test this prediction, we performed voltage-clamp recordings from pairs of MNs during fictive swimming. As expected (*12*, *13*), all MNs received barrages of excitatory postsynaptic currents (EPSCs) in phase with ipsilateral motor activity (Fig. 1A). To evaluate whether these barrages, which are synchronous on a large temporal scale (tens of ms), were derived from a shared premotor network, we assessed whether they were also synchronous at a fine temporal scale (tens of μs) (*14*).

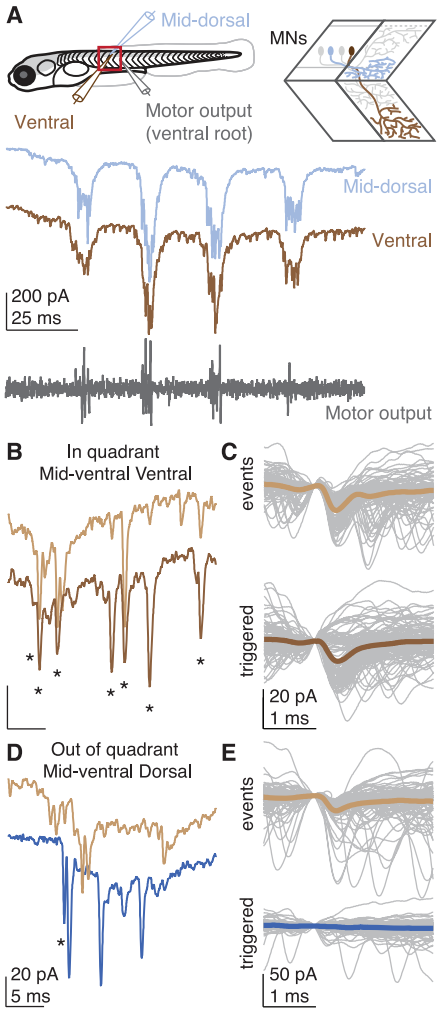

In pairs of MNs innervating the same muscle quadrant, EPSCs during fictive swimming were indeed highly synchronous (Fig. 1B), as exemplified by an overlay of 100 consecutive EPSCs from one neuron and the associated EPSC-triggered average in the other (Fig. 1C). Unexpectedly, excitatory inputs to MN pairs innervating different muscle quadrants lacked synchrony at fine time scales (Fig. 1D), with accordingly small EPSC-triggered average responses (Fig. 1E). Analysis of all data revealed significantly larger EPSC-triggered averages for "in quadrant" (i.e., either dorsal/mid-dorsal or ventral/mid-ventral pairs), as opposed to "out-of-quadrant," pairs (Fig. 1F). Similarly, a measure of event cross-correlation scores for the pooled data revealed a significant peak at 0 ms for in-quadrant versus out-of-quadrant pairs (Fig. 1G) (see also materials and methods and figs. S1 and S2). The low synchrony for out-of-quadrant pairs is incompatible with the

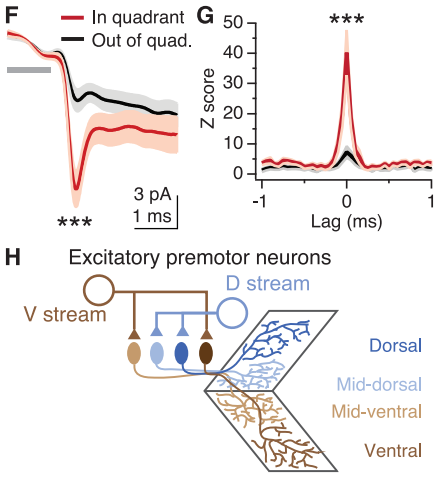

Fig. 1. Distinct excitatory microcircuits govern dorsal and ventral musculature. (**A**) (Top) Recording setup with schematic of example primary MN axon arbors in the musculature. (Bottom) Dual whole-cell recording of EPSCs during swimming from MNs projecting to mid-dorsal and ventral territory. Traces vertically offset for clarity. Simultaneous ventral root recording (gray) shows that excitatory barrages occur in phase with the ipsilateral fictive bend. (**B**) Expanded time scales for EPSCs recorded during swimming from example in-quadrant (mid-ventral and ventral) MNs (Fig. 1H). Asterisks indicate synchronous EPSCs in both neurons [time difference (Δt) < 150 μs]. Scale as in (D). (**C**) One hundred consecutive EPSCs recorded in the mid-ventral MN (gray, top; average in light brown) and simultaneously recorded signals in the ventral MN (gray, bottom) reveal a notable EPSC-triggered average (dark brown). (**D** and **E**) As for (B) and (C) for an example out-of-quadrant (mid-ventral and dorsal) MN pair, revealing few synchronous EPSCs and a small EPSC-triggered average (dark blue). (**F**) Summary EPSC-triggered averages, means ± SEMs, for in-quadrant (n = 15) and out-of-quadrant (n = 19) MN pairs. ***P < 0.001, unpaired t test of peak EPSC amplitude. Gray bar indicates period of baseline normalization. (**G**) Cross-correlogram of EPSC timing, averages from all MN pairs. Means ± SEMs; bin = 50 μs, n as in (F). ***P < 0.001, unpaired t test at 0 ms. (**H**) Schematic of proposed premotor excitatory circuitry. An individual excitatory premotor neuron (open circles) preferentially synapses on either dorsal (D)– or ventral (V)–projecting MNs (solid lines) but not both.

Department of Neurobiology, Northwestern University, Evanston, IL 60208, USA.

*Corresponding author. E-mail: david-mclean@northwestern.edu

assumption that dorsal- and ventral-projecting MNs are embedded in a shared presynaptic network. Instead, premotor excitatory inputs are segregated into two largely distinct microcircuits governing dorsal and ventral musculature (Fig. 1H).

Are inhibitory premotor pathways similarly segregated? On a longer time scale, barrages of inhibitory postsynaptic currents (IPSCs) recorded in two MNs during fictive swimming occurred synchronously, predominantly out of phase with the motor output (Fig. 2A). Similar to EPSCs, at fine temporal scales in-quadrant pairs exhibited strong synchrony of IPSCs and a large IPSC-triggered average (Fig. 2, B and C), whereas out-of-quadrant MN pairs revealed weaker evidence for IPSC correlation and smaller IPSC-triggered averages (Fig. 2, D and E). These observations were borne out by analysis of group data, showing that in-quadrant pairs exhibited a ~2.3-fold larger IPSC-triggered average (Fig. 2F) and twice the magnitude of cross-correlation at 0 ms (Fig. 2G; see also fig. S2) as out-of-quadrant pairs. Thus, similar to premotor excitatory networks, premotor inhibitory networks are also segregated into two distinct microcircuits for the differential control of dorsal and ventral musculature, although the smaller magnitude difference between in-quadrant and out-of-quadrant cross-correlograms (compare Figs. 1G and 2G) suggests, as a conservative estimate, less-stringent specificity for inhibitory connectivity (Fig. 2H).

In mammalian cortex, pyramidal neurons that receive shared excitatory inputs are also more likely to be connected to each other (*14*). Similarly, there is preferential gap junctional coupling between mammalian limb MNs of shared modular function, for example, ankle flexors (*15*). We found that electrical coupling between MNs was twofold higher for in-quadrant as compared with out-of-quadrant pairs (fig. S3). Thus, the segregated microcircuits at the premotor level are supported by increased connectivity among MNs themselves.

To assess whether excitatory segregation derives from spinal sources and to identify specific premotor populations of relevance, we used an optogenetic approach to selectively drive firing in the V2a population expressing the transcription factor *Chx10* (Fig. 3A and fig. S4). V2a/*Chx10*+ neurons are the largest class of ipsilaterally projecting glutamatergic premotor neurons in the spinal cord and have a conserved function during locomotion in both zebrafish and mice (*16*, *17*). Subsequent recording from MN pairs revealed that the EPSCs elicited by pulses of illumination were highly synchronous between in-quadrant pairs (Fig. 3B) but asynchronous between out-of-quadrant pairs (Fig. 3C). Analysis of group data showed that EPSC-triggered averages were 15-fold larger for in-quadrant than out-of-quadrant MN pairs (Fig. 3D). Thus, V2a/*Chx10*+ neurons in the spinal cord are segregated into two subtypes, yielding distinct excitatory control over dorsal and ventral musculature.

Premotor inhibition can derive from both ipsilateral and contralateral spinal sources. Are

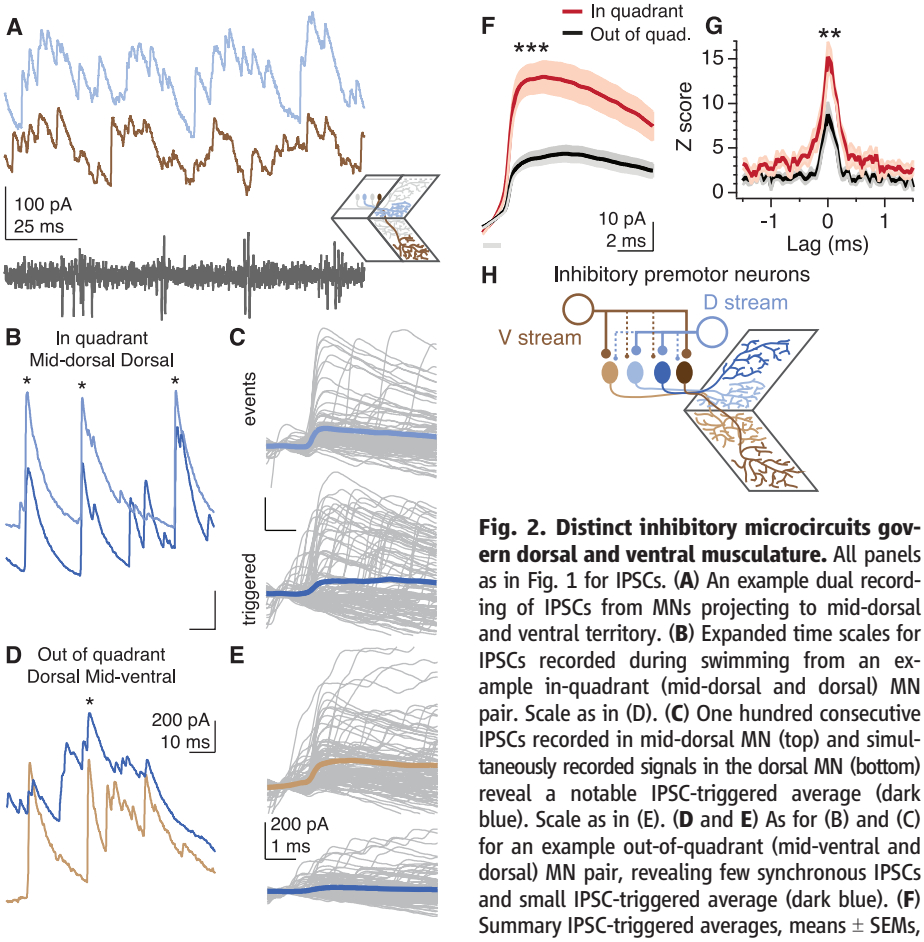

Fig. 2. Distinct inhibitory microcircuits govern dorsal and ventral musculature. All panels as in Fig. 1 for IPSCs. (**A**) An example dual recording of IPSCs from MNs projecting to mid-dorsal and ventral territory. (**B**) Expanded time scales for IPSCs recorded during swimming from an example in-quadrant (mid-dorsal and dorsal) MN pair. Scale as in (D). (**C**) One hundred consecutive IPSCs recorded in mid-dorsal MN (top) and simultaneously recorded signals in the dorsal MN (bottom) reveal a notable IPSC-triggered average (dark blue). Scale as in (E). (**D** and **E**) As for (B) and (C) for an example out-of-quadrant (mid-ventral and dorsal) MN pair, revealing few synchronous IPSCs and small IPSC-triggered average (dark blue). (**F**) Summary IPSC-triggered averages, means ± SEMs, for in-quadrant (n = 13) and out-of-quadrant (n = 17) MN pairs. ***P < 0.001, unpaired t test of peak IPSC amplitude. (**G**) Cross-correlogram of IPSC timing, averages from all MN pairs. Means ± SEMs; bin = 50 μs, n as in (F). **P < 0.01, unpaired t test at 0 ms. (**H**) Schematic of proposed premotor inhibitory circuitry. An individual inhibitory premotor MN preferentially synapses either on D or V MNs (solid lines) but rarely on both (dotted lines).

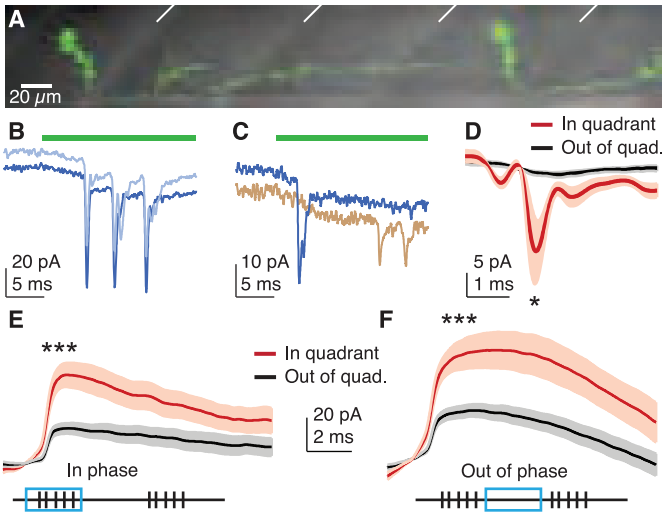

Fig. 3. Intraspinal premotor inputs are segregated into dorsal and ventral microcircuits. (**A**) Sagittal view of 4 days post fertilization (dpf) larva expressing alx:Gal4::UAS:CatCh (see materials and methods for more information) in two premotor neurons with typical V2a morphology (ipsilateral axon, primarily descending). Rostral is to the left; white bars mark muscle segments. (**B**) Example of synchronous EPSCs evoked optogenetically in a dorsal/mid-dorsal MN pair. Green bar indicates light exposure. (**C**) Asynchronous EPSCs evoked in a dorsal/mid-ventral MN pair in another fish. (**D**) Summary of EPSC-triggered averages for in-quadrant and out-of-quadrant MN pairs (n = 5 pairs each). *P < 0.05, unpaired t test of peak amplitudes. Varying baseline period is due to frequent barrages of light-elicited EPSCs [as in (B)]. (**E**) IPSC-triggered average responses in phase with ipsilateral motor activity, as measured by ventral root recordings (schematic, bottom), from in-quadrant (n = 7) and out-of-quadrant (n = 14) pairs. ***P < 0.001, unpaired t test of peak amplitudes. (**F**) As in (E), but for recordings during midcycle, out of phase with ipsilateral motor activity.

both sources of spinal inhibition similarly segregated? We took advantage of the fact that inhibition arriving in phase with the locomotor signal derives exclusively from ipsilateral spinal sources, whereas inhibition arriving out of phase derives from commissural spinal sources (*18*). Both IPSCs occurring in phase and those occurring out of phase with ipsilateral activity exhibited ~2.5-fold larger IPSC-triggered average responses for in-quadrant than for out-of-quadrant pairs (Fig. 3, E and F). We conclude that both ipsilaterally and contralaterally derived spinal inhibitory drive is also segregated into two microcircuits.

To assess the utility of these parallel axial microcircuits for ethologically relevant behaviors, we focused on their recruitment during postural correction, which is known to rely on differential dorsal and ventral muscle activity (*7*, *19*). Normally, a side-lying larval zebrafish will right itself at the beginning of a swim bout (Fig. 4A) (*20*). We quantified the motor activity underlying this behavior by using calcium imaging, which allowed visualization of the activity of the dorsal- and ventral-projecting primary MNs on both sides of the fish (fig. S5A). At the onset of evoked swim bouts, bursts of activity are visible as Ca^{2+} transients (Fig. 4B). In side-lying fish, the amplitude of the Ca^{2+} transient was larger in ventral-projecting than in dorsal-projecting MNs on the ear-up side, but this pattern was inverted on the ear-down side of the fish (Fig. 4C). This asymmetric motor drive thus produces self-righting torque to roll the fish dorsal side up (Fig. 4D) (*7*) and is likely to reflect the overall motor activation pattern in more modest postural correction as well. In contrast, when fish were embedded dorsal side up in a normal orientation, no significant differences were seen in the pattern of activation (fig. S5B).

Is this bias in activity driven by differential excitation or inhibition? Paired physiological recordings from MNs on the ear-up side of side-lying fish revealed that, during swimming, EPSCs were significantly more frequent in ventral-projecting than dorsal-projecting MNs. In addition, IPSCs occurred more frequently in MNs controlling dorsal than ventral musculature (Fig. 4F). Average EPSC and IPSC amplitudes did not differ between the MN types, however (fig. S6).

To test whether vestibular signals were responsible for these asymmetries in behavioral and physiological activity, we evaluated the *rock solo* mutant fish line, in which the anterior otolith [the sole gravity sensor at this stage (*21*)] is absent (*22*). *rock solo* mutant fish failed to develop self-righting during the first week post fertilization, in contrast with their heterozygous and wild-type siblings (13 wild-type or heterozygous fish had 82% successful righting over 49 trials; for 20 *rock solo*, 48% righting, 50 trials; $P < 0.0001$, Fisher exact test). MN imaging in side-lying *rock solo* mutant fish revealed no reliable asymmetry of activity (Fig. 4E), consistent with the absence of self-righting behavior. Similarly, physiological recordings from *rock solo*$^{-/-}$ fish, or from fish in which the otoliths were surgically removed immediately before the experiment to avoid developmental confounds (*23*), revealed no consistent bias for synaptic events in the MNs controlling dorsal and ventral musculature (Fig. 4G).

Critically, however, the differences in EPSC and IPSC synchrony for in-quadrant versus out-of-quadrant pairs persisted in otolith-deficient animals (Fig. 4H). This observation confirms that spinal axial microcircuitry exhibits segregated, modular connectivity to different motor pools even in the absence of structured descending vestibular signals. Collectively, our findings challenge the traditional view of axial network organization (*12*, *13*, *24*) and shift the locus of distinct dorsal or ventral control in fish from supraspinal regions to modular, intrinsic spinal circuits.

The evolution of vertebrates from fishes to mammals involved fundamental changes in body plan, muscle distribution, and posture (*25*). These changes involved not only reorganization of the trunk musculature but also an increasing reliance on the limbs to locomote (*26*). Commensurate with these changes, locomotor networks in the spinal cord must have adapted. Studies of the molecular mechanisms responsible for generating spinal locomotor circuitry have identified conserved programs regulating the differentiation of axial and limb spinal microcircuitry (*27*, *28*).

Although limb microcircuits must have originated from more primitive axial ones, it is unclear

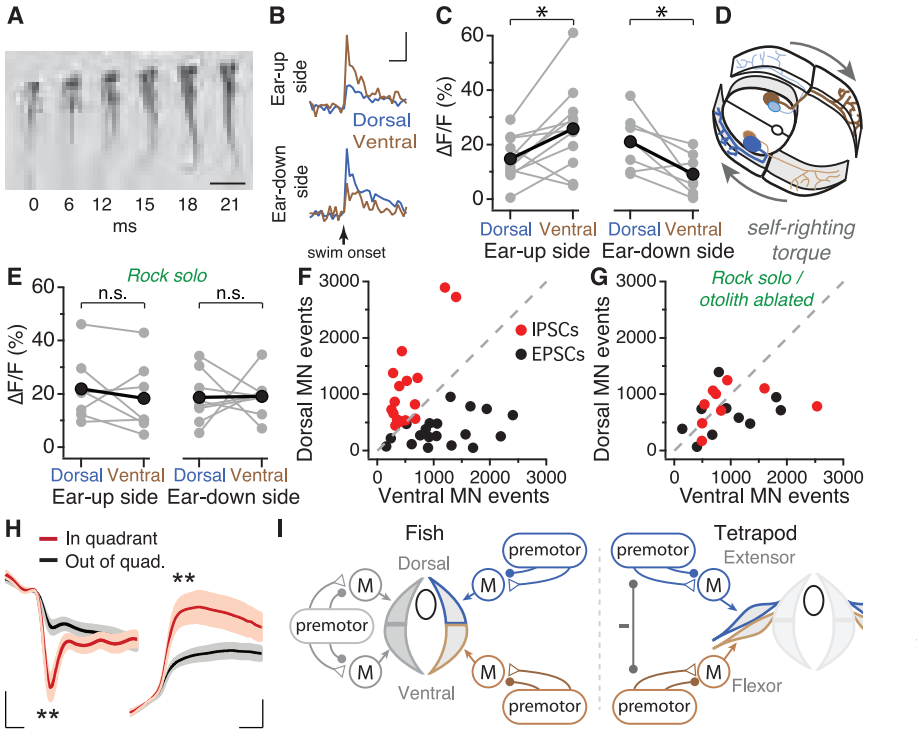

Fig. 4. Descending vestibular information differentially recruits dorsal and ventral microcircuits. (**A**) Time-lapse images of a 3-dpf larva engaging in self-righting from right ear up to dorsal-up orientation. Pictures were taken under normal illumination for display purposes only; behavioral data were gathered with infrared illumination. Scale bar, 1 mm. (**B**) Example Ca^{2+} imaging data from primary MNs in one segment of a side-lying fish. Arrow indicates time of brief electrical stimulus applied to tail to induce swimming. Scale bars, 20% $\Delta F/F$ (where F is fluorescence signal), 5 s. (**C**) Ventral-projecting MNs exhibit larger Ca^{2+} signals than dorsal-projecting MNs on ear-up side (left; $n = 13$ MN pairs from nine fish); pattern is reversed on ear-down flank (right; seven pairs from seven fish). *$P < 0.05$, paired t test. (**D**) Schematic of asymmetric drive to the four quadrants of musculature, producing torque for self-righting. (**E**) Ca^{2+} imaging summary as in (D), for *rock solo* mutant animals (ear-up, $n = 7$ pairs from seven fish; ear-down, $n = 8$ pairs from eight fish). n.s., not significant, paired t test. (**F**) Physiological recordings from MN out-of-quadrant pairs on the ear-up side of wild-type (WT) animals during fictive swimming reveal that EPSCs are more frequent in ventral-projecting MNs than dorsal ($P < 0.001$, paired t test, $n = 19$ pairs), whereas IPSCs are more frequent in dorsal-projecting MNs than ventral ($P < 0.001$, 17 pairs). Each dot represents either EPSC or IPSC data from a single out-of-quadrant pair. Unity line is shown in dashed gray. (**G**) As in (F), for vestibular-deficient animals. No differences are seen in the number of EPSCs ($P = 0.11$, $n =$ 10 pairs) or IPSCs ($P = 0.50$, $n = 9$ pairs) between dorsal- and ventral-projecting MNs. (**H**) Higher in-quadrant than out-of-quadrant synchrony persists in *rock solo* mutants and otolith-ablated animals for both EPSCs and IPSCs. **$P < 0.01$, unpaired t test of peak amplitude (EPSCs, $n = 6$ in-quadrant, 10 out-of-quadrant pairs; IPSCs, $n = 6$ in-quadrant, 9 out-of-quadrant pairs). Scale bars: 4 pA, 0.5 ms; 10 pA, 1.5 ms. (**I**) Schematic summary of results: prior models of a single premotor circuit for dorsal and ventral control in fish (left); current model supporting parallel, modular microcircuits (middle); and proposed homology to limb control in tetrapods (right). M, motor.

how the modular organization of limb networks could have arisen from a single, homogeneous axial network (*5*). Our work demonstrates that axial networks, like limb networks, are organized in a modular fashion to facilitate differential control of muscles during locomotor-related behaviors such as postural correction (*29*). Thus, the modular organization of axial locomotor control systems may have served as a functional template for the evolution of limb control systems (Fig. 4I). We suggest that refinement and reweighting of inhibition between these modules is a plausible candidate mechanism for generating new locomotor patterns from ancient axial circuits.

References and Notes

1. T. G. Deliagina, P. V. Zelenin, G. N. Orlovsky, *Curr. Opin. Neurobiol.* **22**, 646–652 (2012).
2. A. Büschges, *Curr. Opin. Neurobiol.* **22**, 602–608 (2012).
3. M. Hägglund *et al.*, *Proc. Natl. Acad. Sci. U.S.A.* **110**, 11589–11594 (2013).
4. S. Grillner, *Physiol. Rev.* **55**, 247–304 (1975).
5. S. Grillner, T. M. Jessell, *Curr. Opin. Neurobiol.* **19**, 572–586 (2009).
6. A. Kozlov, M. Huss, A. Lansner, J. H. Kotaleski, S. Grillner, *Proc. Natl. Acad. Sci. U.S.A.* **106**, 20027–20032 (2009).
7. P. V. Zelenin, G. N. Orlovsky, T. G. Deliagina, *J. Neurosci.* **27**, 1024–1032 (2007).
8. M. Westerfield, J. V. McMurray, J. S. Eisen, *J. Neurosci.* **6**, 2267–2277 (1986).
9. E. Menelaou, D. L. McLean, *J. Neurosci.* **32**, 10925–10939 (2012).
10. D. L. McLean, J. Fan, S. Higashijima, M. E. Hale, J. R. Fetcho, *Nature* **446**, 71–75 (2007).
11. D. L. McLean, M. A. Masino, I. Y. Koh, W. B. Lindquist, J. R. Fetcho, *Nat. Neurosci.* **11**, 1419–1429 (2008).
12. S. Grillner, *Neuron* **52**, 751–766 (2006).
13. A. Roberts, W. C. Li, S. R. Soffe, *Front. Behav. Neurosci.* **4**, 16 (2010).
14. Y. Yoshimura, J. L. Dantzker, E. M. Callaway, *Nature* **433**, 868–873 (2005).
15. K. D. Walton, R. Navarrete, *J. Physiol.* **433**, 283–305 (1991).
16. Y. Kimura, Y. Okamura, S. Higashijima, *J. Neurosci.* **26**, 5684–5697 (2006).
17. S. A. Crone *et al.*, *Neuron* **60**, 70–83 (2008).
18. A. Roberts, W. C. Li, S. R. Soffe, *J. Comp. Physiol. A* **194**, 185–193 (2008).
19. C. M. Rovainen, *J. Neurophysiol.* **42**, 745–766 (1979).
20. F. Ullen, T. G. Deliagina, G. N. Orlovsky, S. Grillner, *J. Exp. Biol.* **198**, 665 (1995).
21. B. B. Riley, S. J. Moorman, *J. Neurobiol.* **43**, 329–337 (2000).
22. W. Mo, F. Chen, A. Nechiporuk, T. Nicolson, *BMC Neurosci.* **11**, 110 (2010).
23. T. Kohashi, N. Nakata, Y. Oda, *J. Neurosci.* **32**, 5810–5820 (2012).
24. A. J. Ijspeert, A. Crespi, D. Ryczko, J. M. Cabelguen, *Science* **315**, 1416–1420 (2007).
25. N. Schilling, *Front. Zool.* **8**, 4 (2011).
26. H. M. King, N. H. Shubin, M. I. Coates, M. E. Hale, *Proc. Natl. Acad. Sci. U.S.A.* **108**, 21146–21151 (2011).
27. S. Arber, *Neuron* **74**, 975–989 (2012).
28. M. Goulding, *Nat. Rev. Neurosci.* **10**, 507–518 (2009).
29. A. Miri, E. Azim, T. M. Jessell, *Neuron* **80**, 827–834 (2013).

Acknowledgments: We are grateful to E. Cadoff and S. Kishore for generating DNA constructs; E. Cadoff for behavioral experiments; and the McLean lab, E. B. Han, G. B. Edgerton, J. Fetcho, M. Scanziani, M. E. Hale, and M. A. MacIver for feedback on the manuscript. *rock solo* fish were a gift from T. Nicolson; the CatCh construct was a gift from E. Bamberg. Funding for these experiments came from NIH grants K99 DC012536 (M.W.B.) and R01 NS067299 (D.L.M.) Additional support was provided by the Esther A. and Joseph Klingenstein Fund, the Searle Scholars Program, and the Alfred P. Sloan Foundation (D.L.M.). The authors declare no competing financial interests.

Supplementary Materials

www.sciencemag.org/content/343/6167/197/suppl/DC1
Materials and Methods
Figs. S1 to S6
References (*30*, *31*)

6 September 2013; accepted 26 November 2013
10.1126/science.1245629

Apical Abscission Alters Cell Polarity and Dismantles the Primary Cilium During Neurogenesis

Raman M. Das and Kate G. Storey*

Withdrawal of differentiating cells from proliferative tissue is critical for embryonic development and adult tissue homeostasis; however, the mechanisms that control this cell behavior are poorly understood. Using high-resolution live-cell imaging in chick neural tube, we uncover a form of cell subdivision that abscises apical cell membrane and mediates neuron detachment from the ventricle. This mechanism operates in chick and mouse, is dependent on actin-myosin contraction, and results in loss of apical cell polarity. Apical abscission also dismantles the primary cilium, known to transduce sonic-hedgehog signals, and is required for expression of cell-cycle-exit gene p27/Kip1. We further show that N-cadherin levels, regulated by neuronal-differentiation factor Neurog2, determine cilium disassembly and final abscission. This cell-biological mechanism may mediate such cell transitions in other epithelia in normal and cancerous conditions.

Newborn neurons detach an apical cell-process from the ventricular surface and then migrate to the lateral neural tube or to form cortical layers within the brain (*1*, *2*). This step is required for the generation of neuronal and tissue architecture (*2*, *3*), and its failure leads to human periventricular heterotopia (*4*). Down-regulation of N-cadherin is associated with this event (*3*, *5*), as is loss of apical complex proteins (*6*, *7*). The latter may be mediated by down-regulation; protein modification/degradation or relocalization; or loss of apical membrane.

Neural Development Group, Division of Cell and Developmental Biology, College of Life Sciences, University of Dundee, Dundee DD1 5EH, UK

*Corresponding author. E-mail: k.g.storey@dundee.ac.uk

To investigate cell behavior underlying neuron birth, we labeled membranes of individual cells by mosaic transfection of green fluorescent protein– glycosylphosphatidylinositol (pCAGGS-GFP-GPI) into the chick embryonic spinal cord (*8*). We then monitored neurogenesis in ex vivo embryo slice cultures (*1*) using wide-field time-lapse microscopy (*8*). Newborn neurons have a basally located cell body and extend a long, thin cell-process to the apical/ventricular surface. Movies of such cells revealed that shedding of the apical-most cell membrane preceded withdrawal of this cell-process (Fig. 1A). This event, which we name apical abscission, takes ~1 hour (56 min, SD = 18 min, n = 21 cells). It begins with formation of a bulb-like "bouton," followed by subapical constriction, membrane thinning, and eventual abscission, after which the apical cell-process withdraws (42 abscising cells in 34 embryos; all stages observed in 21 cells) (Fig. 1A, fig. S1, and movies S1 to S3). Abscised particles tracked so far remain at the ventricle.

Using structured illumination microscopy (*8*) to generate super-resolution images of abscising cells transfected with membrane-localized Tag–red fluorescent protein–Farnesyl (TagRFP-Farn) revealed a thin membranous connection between apical cell-process and the abscising particle. This confirmed the existence of abscission events in fixed tissue not subject to culture and imaging regimes (n = 5 cells in 3 embryos) (fig. S2 and movie S4). We also observed apical abscission in completely unmanipulated embryos fixed and labeled to reveal the early neuronal marker Tuj1 (class III beta-tubulin). Some Tuj1$^+$ cells with a basally localized nucleus and a ventricle-contacting apical cell-process were found to have a distinct constriction, coincident with subapical actin (n = 31 of 78 cells in 5 embryos) (Fig. 1B and movie S5). To characterize the abscised membrane, we assessed localization of endogenous apical Par-complex protein, atypical protein kinase C (aPKC) (*9*) in such Tuj1$^+$ cells; aPKC was confined to the abscising particle (n = 31 of 31 cells in 5 embryos) (Fig. 1B and movie S5). This indicates that differentiating neurons experience rapid loss of apical polarity. It is also consistent with the absence of Par-complex proteins from withdrawing cell-processes (*6*, *7*), which, now liberated from apical-junctional complexes, extend transient membrane protrusions (18 cells in 9 embryos) (e.g., see movies S1 and S2). Similar apical constrictions were visible in Tuj1$^+$ ventricle-contacting cells in mouse spinal cord (22 of 40 cells in 4 embryos) (Fig. 1C and movie S6),

Modular Organization of Axial Microcircuits in Zebrafish
Martha W. Bagnall and David L. McLean
Science **343**, 197 (2014);
DOI: 10.1126/science.1245629

Science (print ISSN 0036-8075; online ISSN 1095-9203) is published weekly, except the last week in December, by the American Association for the Advancement of Science, 1200 New York Avenue NW, Washington, DC 20005.